

State of the Art Rotordynamic Analyses of Pumps

Frédéric Gaulard¹, Joachim Schmied², Andreas Fuchs³

¹Delta JS AG, 8005, Zurich, Switzerland, fgaulard@delta-js.ch

²Delta JS AG, 8005, Zurich, Switzerland, jschmied@delta-js.ch

³Delta JS AG, 8005, Zurich, Switzerland, afuchs@delta-js.ch

Abstract

State of the art analyses for the rotordynamic assessment of pumps and specific requirements for the simulation tools are described. Examples are a horizontal multistage pump with two fluid film bearings in atmospheric pressure, a horizontal submerged multistage pump with many bearings and a submerged vertical single-stage pump with water lubricated bearings.

Due to the seals the rotor of the horizontal pump on two bearings is statically overdetermined and the static bearing forces depend on the deflection in the seals and the bearing. The nonlinear force displacement relation in the bearings hereby is considered.

The stability of pumps is assessed by Campbell diagrams considering linear seal and bearing properties. Cylindrical bearings can have a destabilising effect in case of low loads as in the examples of the submerged pumps.

For the pump with many bearings the influence of the bearing ambient pressure and of the bearing specific load on the stability is analysed.

For the vertical pump the limit cycle, i.e. the vibration level of stabilisation, is determined with a nonlinear analysis.

All examples have a practical background from engineering work, although they do not exactly correspond to real cases. Analyses were performed with the rotordynamic software MADYN 2000 [1].

1 Introduction

Fluid-rotor interaction plays a big role in the rotordynamics of pumps. The forces in small clearances, i.e. at the seals and bearings, have the largest impact. The seal forces can have a destabilising effect, but also a stiffening effect (Lomakin) and thus contribute to carrying the weight load.

There is a long history of research on the impact of seals and complete impellers in rotordynamics. They are typically considered by rotordynamic stiffness, damping and mass coefficients. A good summary of activities can be found in the book of Dara Childs [2].

Special requirements for rotordynamic analyses due to the seals are described in this paper for the example of a horizontal pump in atmospheric pressure.

Fluid film bearings have a long history in research as well. Famous researchers are Glienicke [3] and Lund [4]. In 1994 2-phase flow was introduced [5] as a new cavitation model. It allows better describing the properties of a mixture of oil and gas as well as considering the influence of elevated environmental pressure on cavitation. At high pressure it is suppressed completely (so called Sommerfeld boundary condition).

In submerged pumps the bearings are lubricated by the process fluid and are in a pressurised environment. Suppression of cavitation therefore plays a big role in these machines. This leads to surprising behaviour, different from the normal behaviour of bearings in atmospheric pressure environment. Many engineers are not aware of this, since so far it is not described in textbooks. The example of a submerged pump describes this behaviour.

Nonlinear fluid film bearing behaviour is an issue for vertical pumps, the third example in this paper. They are typically linearly unstable. A nonlinear analysis allows assessing the vibration level by calculating the limit cycle.

2 Horizontal multistage pump with two bearings at atmospheric pressure

2.1 Description of the model

The model of the centrifugal pump is shown in Figure 1. The rotor has a total length of 1'730mm and a bearing span of 1'330mm. The mass of the rotor is 52kg; its nominal speed is 9'000 rpm. It is supported on two tilting-pads bearings with a diameter of 50mm and a clearance of 2.0‰, which are lubricated with oil type ISO VG46 with an inlet temperature of 50°C. The bearings are analysed as described in [6] with consideration of the 3D distribution of the temperature and viscosity in the fluid film, of the turbulence in the fluid film and of the thermo-elastic deformation of the shaft and pads.

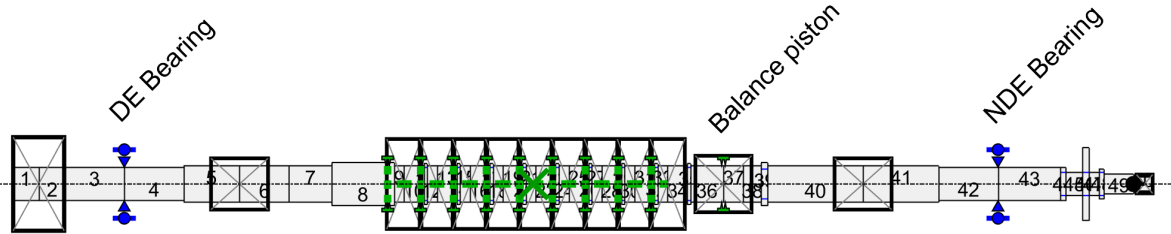


Figure 1: Horizontal multistage pump on two bearings at atmospheric pressure.

The seals at the impeller shrouds and hubs, as well as the balance piston seal are included in the model. The impeller seals are plain annular seals; the balance piston seal is a serrated seal. The seals are analysed with the specialised CFD program SEAL 2D/3D, which was originally developed by Nordmann et. al. (see [7]), further improved for industrial use and integrated into MADYN 2000. The code solves the Navier-Stokes equations with the finite difference method. For the balance piston, the radial and tangential forces as a function of the precession frequency at nominal speed are shown in Figure 2. The calculated points are shown with “Xs”. The speed-dependant linear coefficients, including mass coefficients, are determined by curve fitting (solid lines).

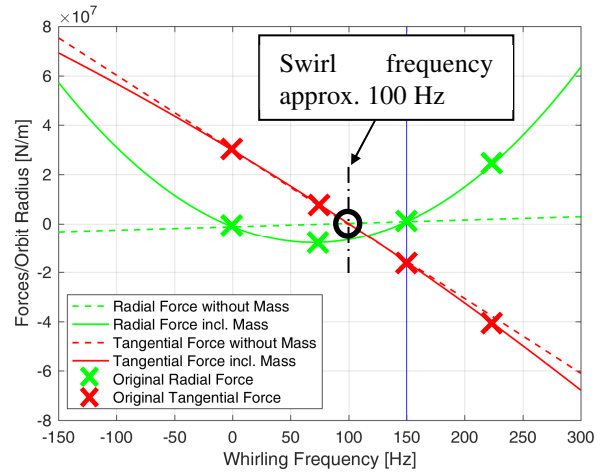


Figure 2: Balance piston seal, forces vs. whirling frequency.

2.2 Static analysis

The static analysis yields the bearing loads, which are needed to determine the load and speed dependent bearing characteristics. The seal forces influence the static equilibrium of the rotor. With a total of 18 seals and 2 bearings the shaft is statically overdetermined. The relation between bearing force and displacement in fluid film bearings is nonlinear. Therefore, a nonlinear static analysis is required. The seal characteristics are assumed as linear, since they have large clearance and cavities.

On some pumps the bearing housings are raised relatively to the pump casing to reduce the static shaft eccentricity at the seal locations. This can be considered in the analysis. In the present example the seal clearances are sufficiently high to avoid rubbing, and the bearing housings were not lifted.

Due to the speed dependence of the seals and bearings the static analysis must be carried out for the whole speed range of interest. The analysis starts with rigid supports instead of the actual bearings (no compliance due to the fluid film), which yields a first estimate of the bearing forces. The journal position in the bearing caused by the bearing force is then calculated yielding a new bearing force and a new position. During each iteration step the bearing code is called with the relevant force and returns the journal position. The iteration stops when the change of force and position in an iteration step is sufficiently small.

In Figure 3 the shaft displacements at nominal speed from two different static analyses are shown. The plot on the left is the result of an analysis where the bearings are modelled as rigid supports and the seal forces are not considered. For the plot on the right the analysis was carried out with consideration of the non-linear bearing characteristics and of the seal forces. The influence of the seals is clearly visible, notably at the balance piston seal, where the shaft is significantly lifted.

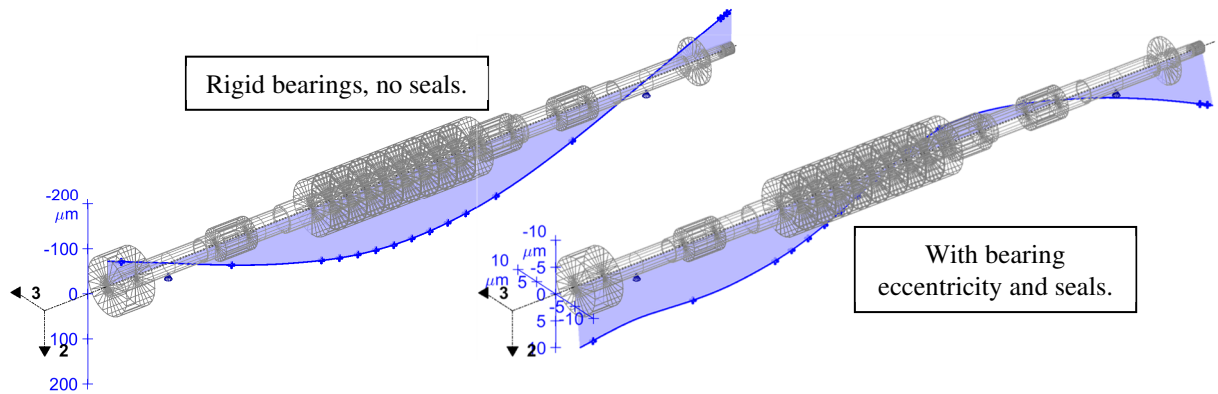


Figure 3: Results of the static analysis, shaft displacement at 9'000rpm.

Plots of the shaft forces can be found in Figure 4. With consideration of the seal forces the bearing loads are much lower.

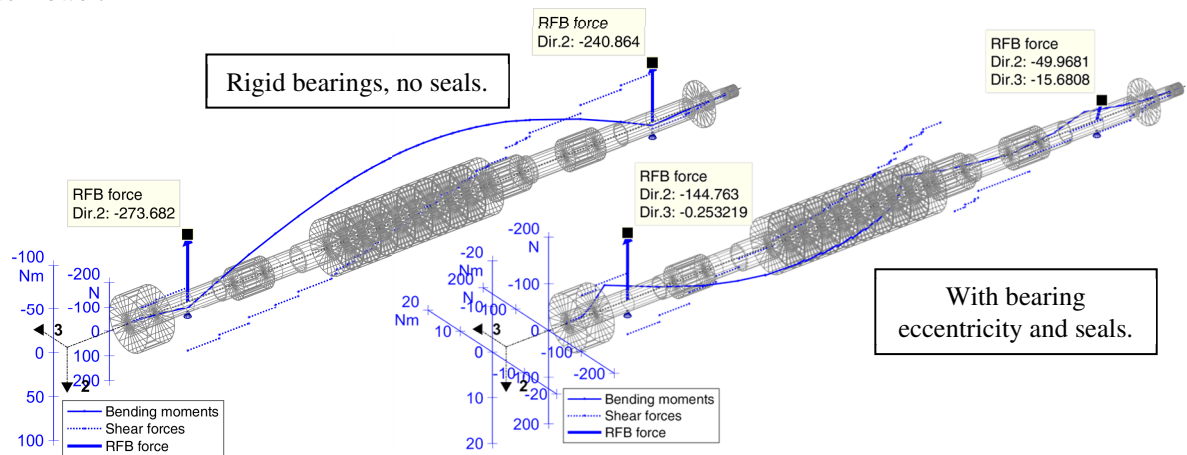


Figure 4: Results of the static analysis, shaft forces at 9'000rpm.

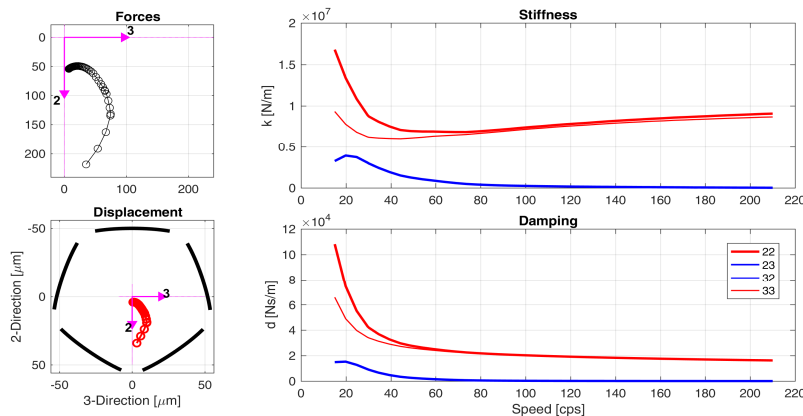


Figure 5: NDE bearing, results of the bearing analysis and linear coefficients.

The speed-dependant bearing forces at the non-drive end bearing (NDE bearing) can be seen in the upper left quadrant of Figure 5. The corresponding displacements are shown in the lower left quadrant. The bearing coefficients can be seen on the right of the figure.

2.3 Campbell Diagram

The Campbell diagram is calculated with the speed dependent bearing loads and speed dependent linear coefficients for the bearings and the seals. It is shown in Figure 6 together with the mode shapes at the critical speeds. In Figure 7 the assessment of the eigenvalues at nominal speed according to API 610 can be found (see [8]). The modes are well damped and smooth operation is expected for this pump.

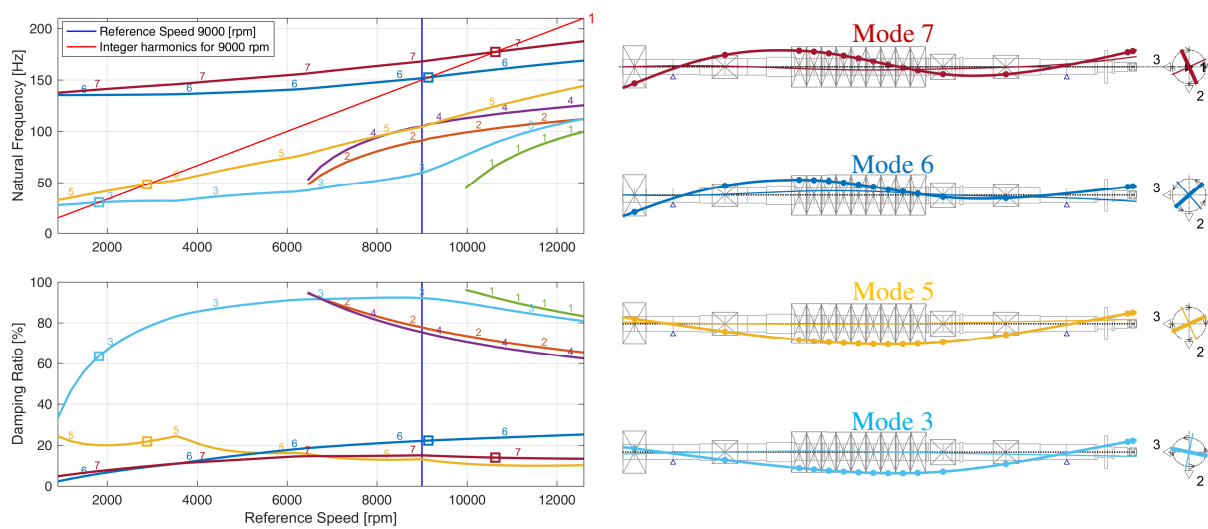


Figure 6: Campbell diagram and critical modes.

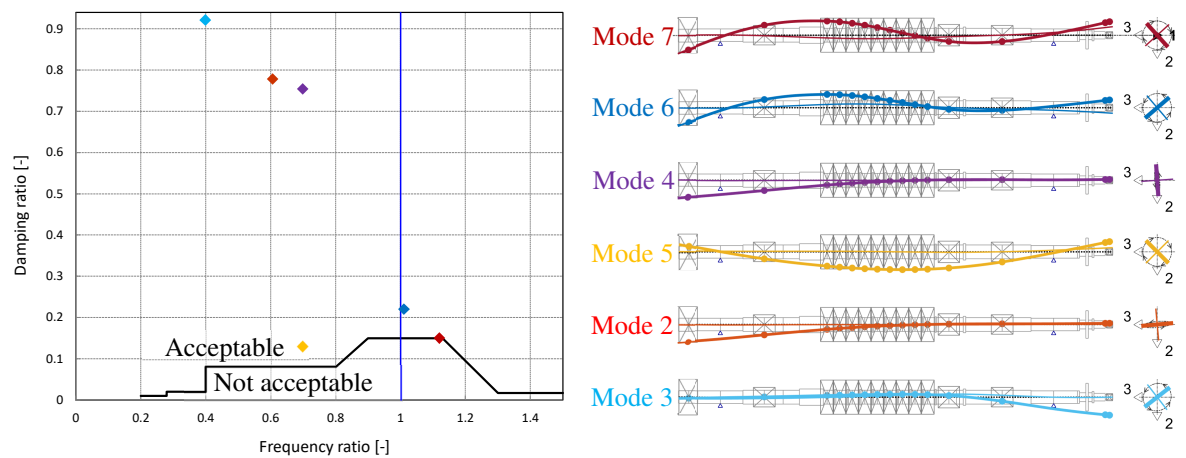


Figure 7: Assessment of the eigenvalues according to API 610 and mode shapes at 9'000 rpm.

3 Submerged horizontal multistage pump with many pressurised bearings

Submerged electrical pumps can have many stages and typically have very elastic shafts. For this reason, they have many bearings. In this section of the paper we look at a sector with a few stages of such a pump to demonstrate some effects, which can occur in such a pump. The whole rotor in such a pump is surrounded by crude oil, which is also used as lubricant for the bearings. In our example the viscosity is 0.1Pa·s at 85°C and the density is 920 kg/m³.

3.1 Description of the model

A plot of the analysed shaft sector can be seen in Figure 8. The shaft diameter is 36mm; the nominal speed is 4'600rpm. The rotor was cut midway between two bearings. At the ends of this shaft sector the added masses used to model the impellers have half the mass of the actual impellers. Quasi-rigid bending springs have been added at the ends of the rotor to calculate the correct bearing loads in the static analysis.

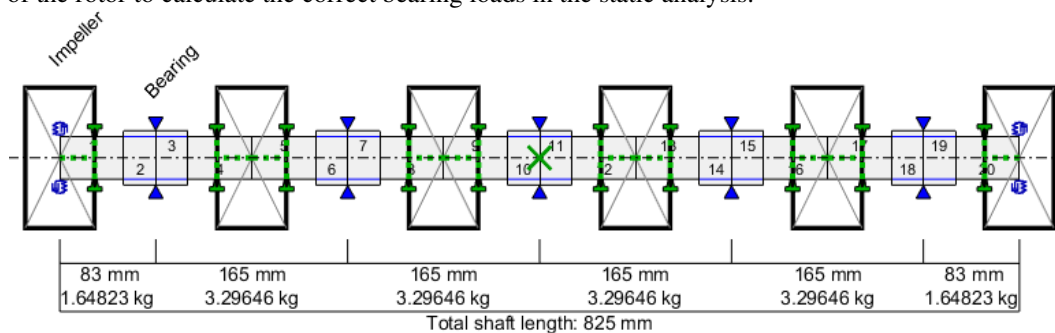


Figure 8: Horizontal multistage pump with many pressurised bearings.

Due to the relatively small impeller head the seal forces are rather small and therefore negligible.

The bearings are closed cylindrical bearings (i.e. cylindrical bearings with one continuous sector between 0° and 360°) with axial oil inlet (pressure difference across the bearing of 2.5bar). The relative bearing clearance is 3‰. The shaft journal is cylindrical, without any axial or helicoidal groove. The bearings are lubricated with the pumped fluid and the ambient pressure increases with each stage (between 107.5bar and 120bar for the present example). The static analysis with weight load was carried out on rigid

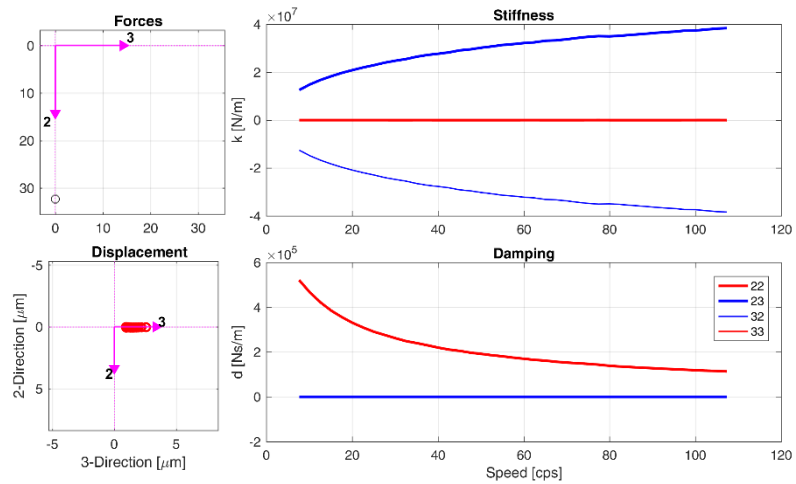


Figure 9: Results of the bearing analysis and linear coefficients.

supports, which is an acceptable simplification for such a flexible rotor supported on so many bearings. The bearing specific load is approximately 0.2bar. The bearings were analysed with consideration of the 2-phase cavitation model described in [6]. Results for the bearing at an ambient pressure of 107.5bar are shown in Figure 9. Typical of a closed cylindrical bearing, the displacement of the journal is perpendicular to the load. The direct stiffness is very small and the cross-coupling stiffness high, which contributes to destabilising the rotor.

3.2 Campbell diagram

The Campbell diagram can be seen in Figure 10. The first mode is the forward whirling parallel mode of the shaft. The other modes are the forward bending modes of the rotor with increasing order and frequency. All modes have circular orbits.

For all modes, the natural frequency is approximately half of the rotating speed, which corresponds to the oil whirling frequency. The damping ratio of the 1st mode is slightly negative (i.e. the mode is unstable). The other modes have positive damping ratios. Modes 3 and higher have high damping ratios.

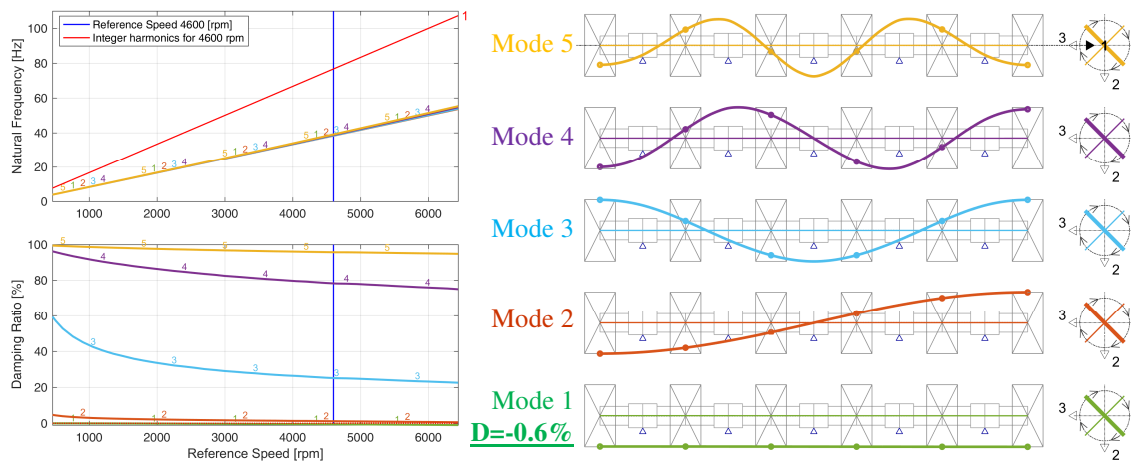


Figure 10: Campbell diagram and mode shapes at 4'600 rpm.

3.3 Influence of the bearing ambient pressure when the bearing specific load is constant

In this section the influence of the ambient pressure on the eigenvalues at nominal speed was analysed. The bearing specific load is kept constant at 0.2bar. The ambient pressure is the same for all bearings and is increased from 1bar (atmospheric pressure) up to 100bar.

The natural frequencies do not change much with the ambient pressure, whereas it has more influence on the damping ratios. In Figure 11 the damping ratios of modes 1 and 2 as a function of the ambient pressure are shown. Between 1bar and approximately 7bar the damping ratios decrease with increasing ambient pressure. Beyond 7bar the influence of the ambient pressure is small.

The bearing coefficients at nominal speed as a function of the ambient pressure can be seen in Figure 12. The direct stiffness coefficients and the cross-coupling damping coefficients causing radial forces decrease with the ambient pressure. At the same time, the cross-coupling stiffness, which tends to destabilise the rotor, increases. The combination of both phenomena contributes to the decrease of damping ratio of the modes when the ambient pressure increases.

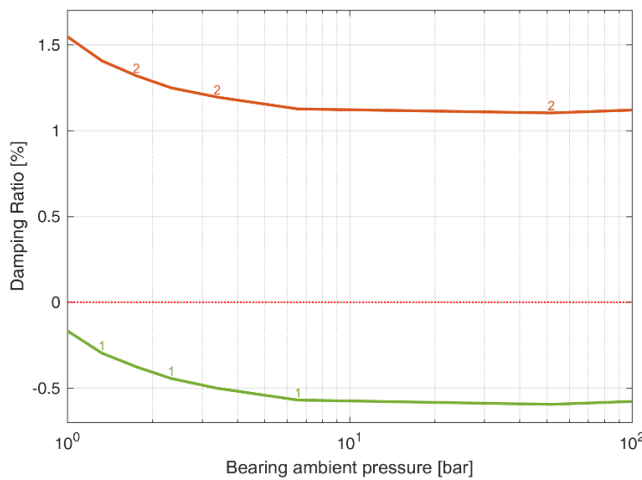


Figure 11: Damping ratio of the 1st and 2nd mode at 4'600 rpm vs. bearing ambient pressure.

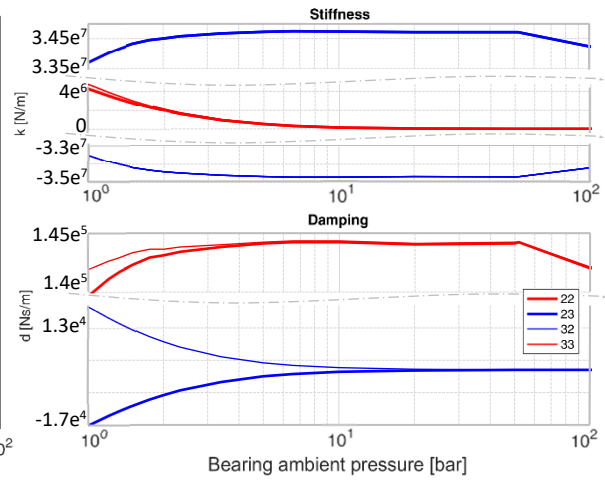


Figure 12: Bearing coefficients vs. ambient pressure

3.4 Influence of the bearing specific load

In this section the influence of the specific bearing load is shown at constant ambient pressure between 107.5bar and 120 bar. The damping ratio of the 1st and 2nd modes as a function of the bearing specific load can be seen in Figure 13. For comparison results with an ambient pressure of 1bar are shown as well. The actual bearing specific load could be increased for example by reducing the number of bearings, reducing the diameter or the width of the bearings or by applying adequate misalignment between the bearings.

When the bearings are at atmospheric pressure, the damping ratios increase with the specific load slowly up to 2.5bar of specific load, and then more rapidly. They can even reach very high values for bearing loads around 10bar. This behaviour is expected for rotors on fluid film bearings and reported in many textbooks.

With pressurised bearings, the damping ratio stays constant as long as the bearing load is lower than 0.56bar and then decreases, which is surprising having the usual behaviour of rotors on fluid film bearings in mind.

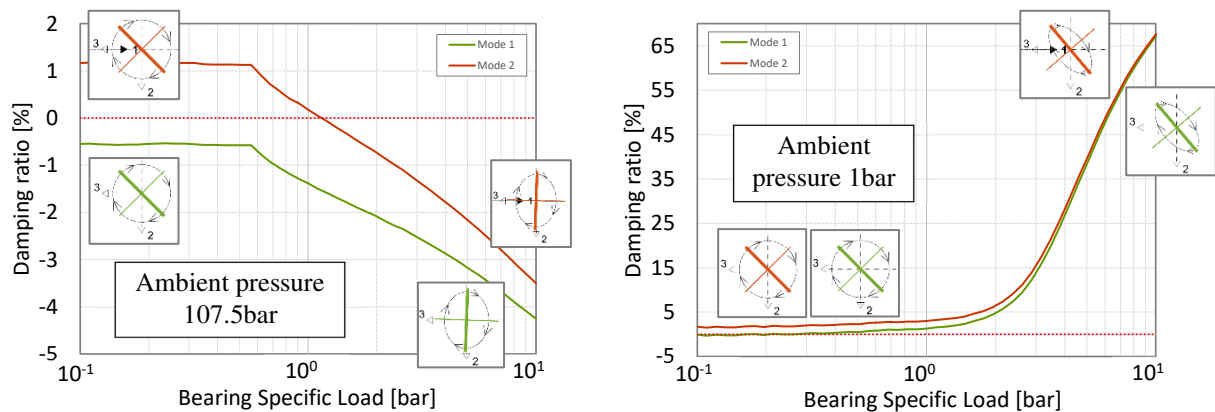


Figure 13: Damping ratio of the 1st and 2nd mode vs. bearing specific load.

The rotordynamic stiffness and damping coefficients for the two cases are shown in Figure 14. It can be clearly seen that the pressurized bearing with increasing bearing load continues to behave like an unloaded cylindrical bearing. The direct stiffness remains small and the destabilising skew symmetric cross coupling stiffnesses are large and increase with the bearing load. The direct damping is also increasing with the load. In contrast to this the direct stiffness increases for the bearing in atmospheric pressure and the stiffness matrix turns into an asymmetric but no longer skew-symmetric matrix.

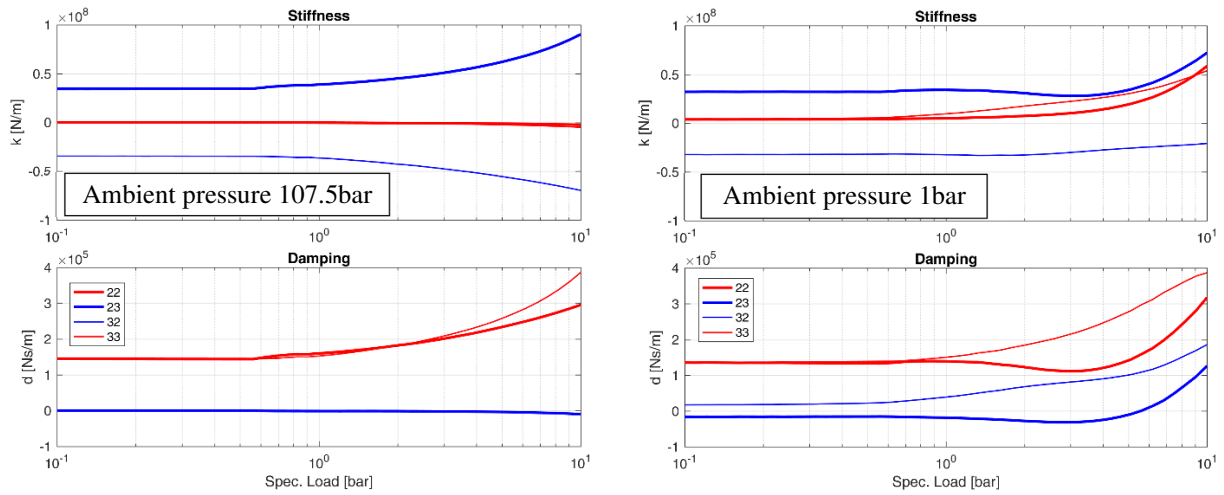


Figure 14: Bearing coefficients vs bearing specific load.

The behaviour can be explained by looking at the pressure distribution and static deflection of the shaft for the two cases: pressurised bearing, bearing in atmospheric pressure.

In Figure 15 the pressure distribution and the oil ratio in the fluid film are shown for the two cases. The axial pressure difference is 2.5 bar. The results are represented in 2D fields where the x-axis is the circumferential angle (0° is at the bottom of the bearing, i.e. in direction 2 of Figure 16) and the y-axis is the axial coordinate. For a given location, an oil ratio 1.0 means that the volume is completely filled with oil; an oil ratio equal to 0 means that the volume is completely filled with air.

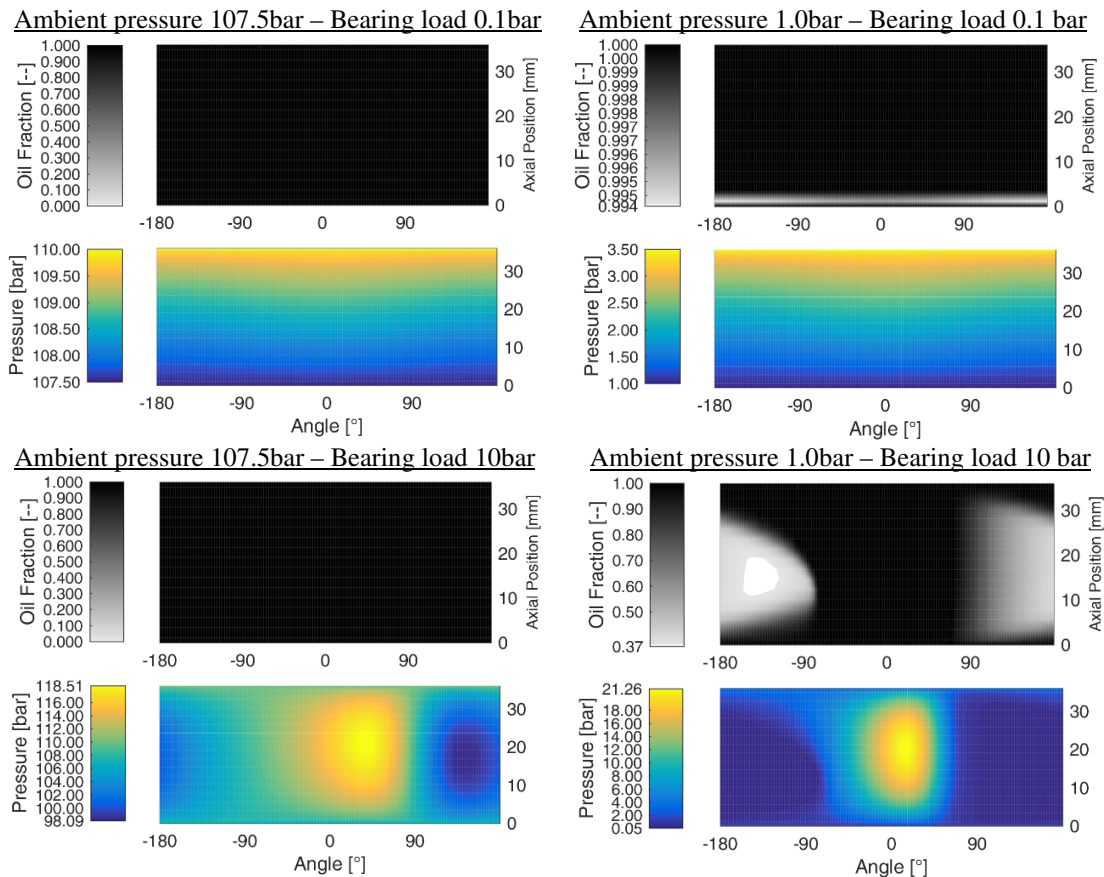


Figure 15: Cavitation area and pressure distribution in the bearing oil film.

With a low specific bearing load of 0.1bar the pressure distributions are rather similar for the two cases. There is no cavitation.

With a specific bearing load of 10bar there is cavitation in the bearing at atmospheric pressure (white area on the oil ratio plot). The pressure peak is narrow in the circumferential direction and centred at about 15° , which is before the angular position of the shaft deflection at about 50° (see Figure 16). This means the peak is before the narrowest gap in the bearing. Cavitation occurs in the upper part of the bearing from 90° to 270° , i.e. -90° .

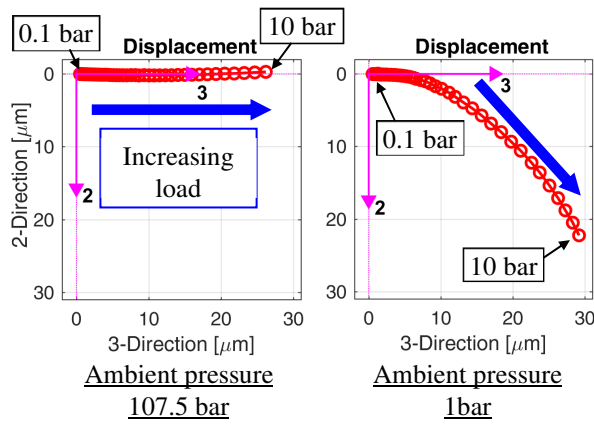


Figure 16: Position of the shaft centreline for increasing bearing specific load.

In the pressurised bearing there is no cavitation at all, the oil ratio is 1.0 everywhere. The region of cavitation at atmospheric pressure now also contributes to carrying the load due to a pressure below the high ambient pressure. Due to the symmetry of the bearing the pressure increase before the narrowest gap and decrease after the narrowest gap must be symmetric to the horizontal 3-direction to get a resulting vertical force carrying the load. This can only be realised by a horizontal deflection.

In Figure 16 can be seen, that for the pressurised bearing the deflection is more or less in horizontal direction (perpendicular to the bearing load), whereas for the bearing in atmospheric pressure it resembles the well-known Gumbel curve, i.e. with increasing load the component of the deflection in load direction increases.

4 Single stage vertical pump with cylindrical water-lubricated bearings

Fluid film bearings are normally linearised around their static load, which yields the linear stiffness and damping coefficients. The linearised behaviour can give good results in a wide range of dynamic loads if the latter do not exceed the static load. If the static load is zero or small, then strictly speaking the behaviour is always nonlinear. A linear analysis does not tell at which level the unstable system stabilises (limit cycle). To get this result, which is essential for an assessment of the rotor behaviour, a nonlinear analysis is necessary. In the following example, which is presented more in detail in [9], the rotor is unstable because it has unloaded cylindrical bearings.

4.1 Description of the model

The model of the vertical pump is shown in Figure 17. The complete length of the assembly is about 12m. The upper part and the motor are on the left side. The pump has only one impeller at the bottom shown on the right side. The pump rotor is shaded in blue. The casing of the pump, which is a pipe, is modelled as a shaft with zero speed. It is shaded in grey (partly visible as a black line). The pipe is fixed to a foundation, which is denoted as customer support in the model. It consists of a flange of the pipe. The flange is fixed with general springs to the ground. The general springs represent the stiffness of the foundation and introduce anisotropy to the system. The motor rotor is not modelled as part of the shaft since it is coupled to the pump shaft with a flexible coupling. The whole motor including its housing is modelled as a rigid mass (the sphere in Figure 17) fixed to the flange at the customer support. The distance of the centre of gravity to the support is bridged with a rigid element.

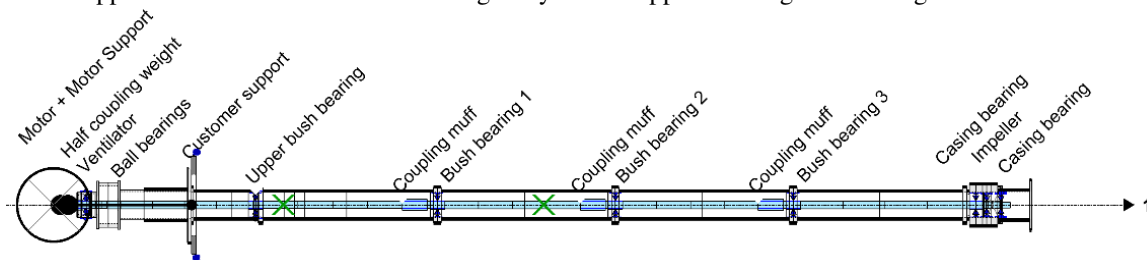


Figure 17: Model of the vertical pump.

The pump shaft is supported in the pipe with an angular contact rolling element bearing, which also carries the axial load, and several bush bearings. The rotor in the pipe is surrounded by pressurised water. Like in the previous example, the elevated ambient pressure and its influence on the cavitation are considered in the bearing analyses with a 2-phase model. The seal located at the impeller is also included in the analysis. Since the relative shaft vibration is relatively small at this location for the dominating modes linear coefficients can be used. The coefficients are applied between the casing and the rotor.

The influence of the water located inside the pipe, which is displaced when the pipe vibrates, is considered by applying an added mass to the pipe (the mass of the enclosed water is added). The water mass displaced by the rotor has a small impact on the dynamics of the shaft line and has been neglected. The influence of the water outside the pipe was not taken into account.

4.2 Linear behaviour, Campbell diagram

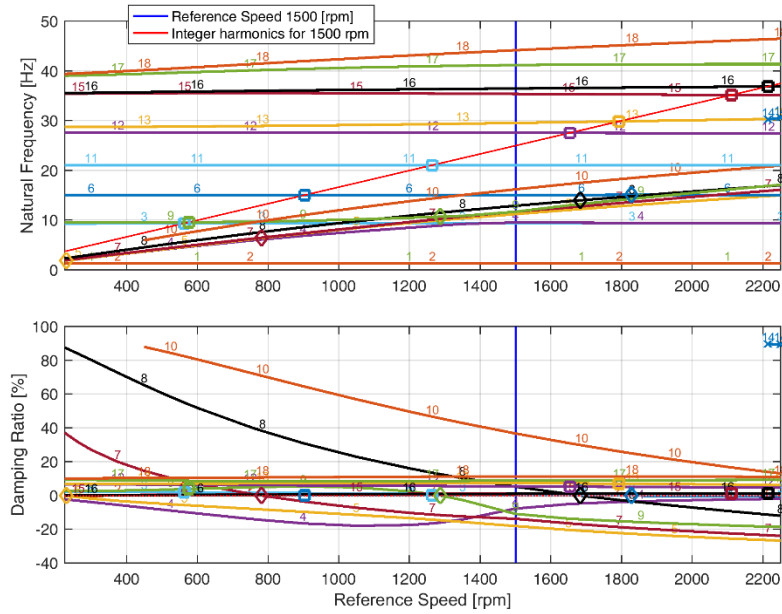


Figure 18: Campbell diagram with eigenvalues.

The Campbell diagram for a speed range up to 150% speed can be seen in Figure 18.

The first two modes are a cantilever-like bending mode of the pipe and the rotor in two perpendicular directions. There is almost no relative displacement between rotor and pipe. The next modes are bending modes of the rotor with increasing order and increasing relative displacement. The modes appear as elliptically forward and backward whirling modes. They are elliptic due to the anisotropy of the support stiffness. The forward modes with relative displacement become unstable (mode 4, 5, 7, 9) when their frequency is below 50% speed, which is the whirling speed of the fluid in the cylindrical bearings.

4.3 Results of a nonlinear run up analysis

The nonlinear models of the fluid film bearings and of the rolling element bearing, as well as the method used to solve the nonlinear equations are presented in detail in [6]. For the present example, a run up with an unbalance of G10 at the impeller has been carried out over a speed range from 10% to 110% speed in 60s, which is almost stationary for this system.

Results of this analysis can be seen in the following figures: The absolute displacements of the pipe at the bearing locations in Figure 19, the orbits of the relative displacements in the fluid bearings in Figure 20 and the 3D shape at 1500rpm in Figure 21.

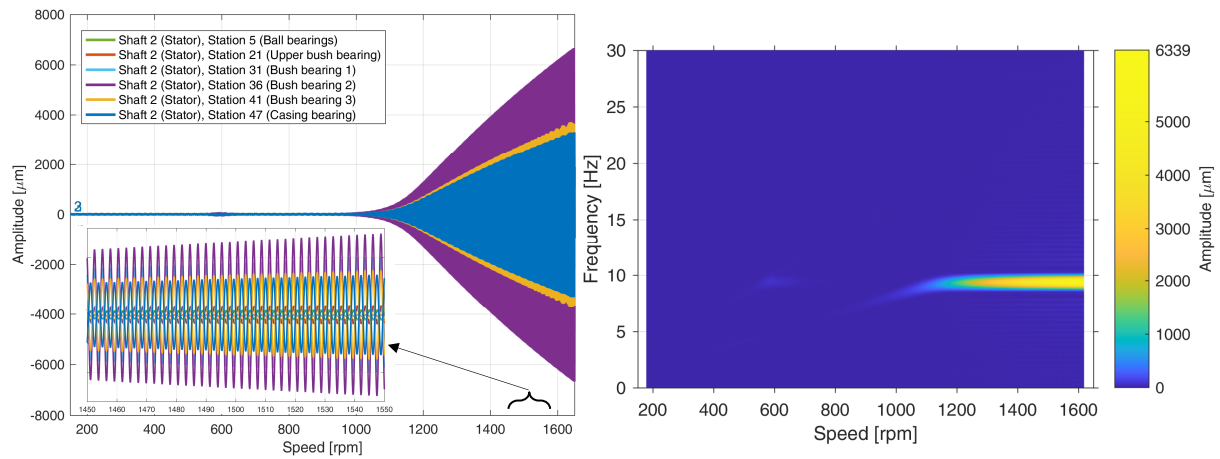


Figure 19. Absolute vibrations of the pipe at the bearing locations.

The vibrations of the pipe indeed are huge. At 100% speed (1'500rpm), the level at bush bearing 2 is several mm. The shape at about 1'500rpm in Figure 21 corresponds to the 2nd bending mode. The by far dominating frequency is about 10Hz, which corresponds approximately to the frequency of this mode. The vibration level at the ball bearing at the top is much lower. At 1'500rpm it is about 300µm, which still corresponds to a high rms value of 33mm/s. This is the location where vibrations of such machines are typically measured. Other locations close to the bearings are difficult to access on such a pump.

The relative vibration level in the fluid bearings at nominal speed in Figure 20 is about 90% of the bearing clearance for all bearings.

The force at nominal speed in bush bearing 2 is about 2'400N, corresponding to a specific dynamic load of 3bar.

The vibration behaviour of the pump as presented here is not acceptable or at least at the limit. The surrounding water, which is not considered in the analysis, probably helps attenuating the vibration, especially at such levels as calculated here.

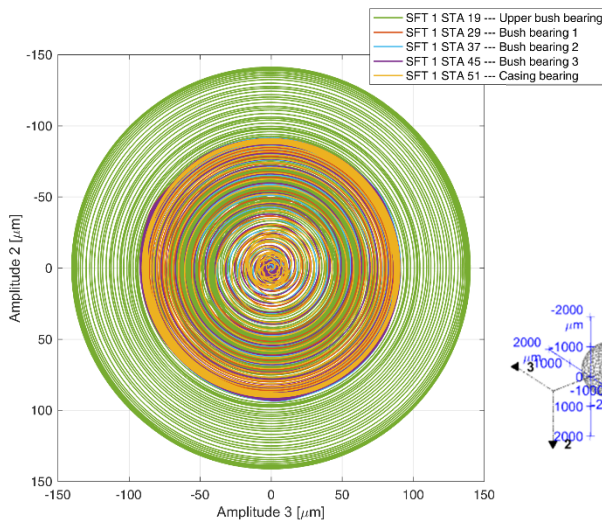


Figure 20: Orbits of relative vibrations in the fluid bearings.

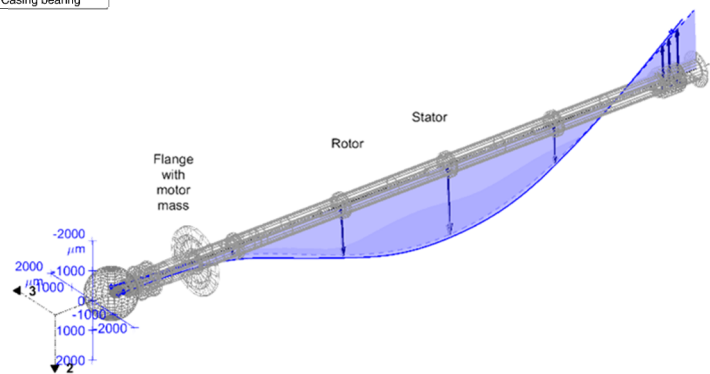


Figure 21: Shape at nominal speed of 1500rpm.

7 Conclusion

Three examples are presented demonstrating requirements for rotordynamic analyses of pumps and typical results.

In a first example the impact of seals on the static deflections and bearing loads as well as on the dynamic behaviour is shown. Due to the seals a simple rotor on 2 bearings turns into a statically overdetermined system.

A second example shows the behaviour of the sector of a submerged pump. The special phenomenon that higher specific bearing load does not lead to a more stable system is shown and explained.

A third example of a vertical pump with the rotor mounted in a pipe filled with water is shown. Limit cycles of the linearly unstable system during run up are calculated in a nonlinear transient analysis.

References

- [1] Schmied, J. (2019): Application of MADYN 2000 to rotor dynamic problems of industrial machinery. Proceedings of SIRM 2019 – 13th International Conference on Dynamics of Rotating Machines, Copenhagen, Denmark.
- [2] Childs D. (1993): *Turbomachinery Rotordynamics*. Wiley Inter Science Publication, New York, Chichester, Brisbane, Toronto, Singapore.
- [3] Joachim Glienicke (1966): *Feder- und Dämpfungskonstanten von Gleitlagern für Turbomaschinen und deren Einfluss auf das Schwingungsverhalten eines einfachen Rotors*. Dissertation, Technische Hochschule Karlsruhe.
- [4] Lund J., Thomsen K. (1978): A Calculation Method and Data for the Dynamics of Oil Lubricated Journal Bearings. *Fluid Film Bearings and Rotor Bearings System Design and Optimization*. ASME, New York (1978), pp. 1-28.
- [5] Xiong Cheng (1994): *Einfluss einer Schmierfilmkavitation auf die dynamischen Eigenschaften von Quetschöldämpfern*. Fortschr.-Ber. VDI Reihe 1 Nr. 243. Düsseldorf, VDI-Verlag.
- [6] Fuchs A. et al. (2015): High Speed Hydrodynamic Bearings – State of the Art Calculations. *Proceedings of SIRM 2015 – 11th Conference on Vibrations in Rotating Machines*, Magdeburg, Germany.
- [7] Nordmann R., Dietzen F. J. (1987): Calculating Rotordynamic Coefficients of Seals by Finite-Difference Techniques. *ASME Journal of Tribology*, July 1987, Vol. 109, pp 388-394.
- [8] API Standard 610: *Centrifugal Pumps for Petroleum, Chemical and Gas Industry Services*, Eleventh Edition, September 2010.
- [9] Schmied J., Fuchs A. (2019): Nonlinear Analyses in Rotordynamic Engineering. *Proceedings of 10th International Conference on Rotor Dynamics – IFToMM*, Vol. 3, pp 426-442.